

# Non-Equilibrium Structural and Dynamic Behaviors of Polar Active Polymer Controlled by Head Activity

Jia-Xiang Li,<sup>1</sup> Li-Li Hao,<sup>2</sup> Song Wu,<sup>1</sup> Qun-Li Lei,<sup>1,\*</sup> and Yu-Qiang Ma<sup>1,†</sup>

<sup>1</sup>*National Laboratory of Solid State Microstructures and School of Physics, Collaborative Innovation Center of Advanced Microstructures, Nanjing University, Nanjing 210093, P. R. China*

<sup>2</sup>*Research Institute for Biomaterials, Tech Institute for Advanced Materials, College of Materials Science and Engineering, Nanjing Tech University, Nanjing 211816, P. R. China*

Thermodynamic behavior of polymer chains out of equilibrium is a fundamental problem in both polymer physics and biological physics. By using molecular dynamics simulation, we discover a general non-equilibrium mechanism that controls the conformation and dynamics of polar active polymer, i.e., head activity commands the overall chain activity, resulting in re-entrant swelling of active chains and non-monotonic variation of Flory exponent  $\nu$ . These intriguing phenomena lie in the head-controlled railway motion of polar active polymer, from which two oppose non-equilibrium effects emerge, i.e., dynamic chain rigidity and the *involution* of chain conformation characterized by the negative bond vector correlation. The competition between these two effects determines the polymer configuration. Moreover, we identify several generic dynamic features of polar active polymers, i.e., *linear* decay of the end-to-end vector correlation function, polymer-size dependent crossover from ballistic to diffusive dynamics, and a polymer-length independent diffusion coefficient that is sensitive to head activity. A simple dynamic theory is proposed to faithfully explain these interesting dynamic phenomena. This sensitive structural and dynamical response of active polymer to its head activity provides us a practical way to control active-agents with applications in biomedical engineering.

**Introduction** The scaling theory of polymer introduced by de Gennes [1] lays the foundation of polymer physics [2, 3]. One of its prediction is the universal scaling behavior of polymer's size, or radius of gyration  $R_g$ , on monomer number  $N$ , i.e.,  $R_g \sim N^\nu$  with  $\nu$  the well-known Flory exponent [4]. For thermal-equilibrated polymer chain, there are three distinct scaling regimes, i.e., polymer in good solvent ( $\nu=0.588$ ), theta solvent ( $\nu=1/2$ ) and bad solvent ( $\nu=1/3$ ). Nevertheless, how the introduction of non-equilibrium effects modifies these classical predictions is an open question relevant to some key biological processes. For examples, bio-polymer like DNA chromatin in nucleus and actin filament of cellular cytoskeleton are subjected to propelling forces from either DNA helicases or motor proteins [5–9], metabolic enzymes can form filamentous membraneless organelles termed cytoophidia that are efficiently transported through complex cellular structures with the help of actin filaments [10, 11]. These active polymers exhibit complicated self-organized structures and abnormal dynamics that challenge classical polymer physics theory [12–18]. On the other side, many artificial active polymers have also been realized, like motility assays of actin filament [19, 20], active colloidal polymers [21–24], actuated mechanical chain/ribbon [25–27], which shows potential application value in drug-delivery and soft-body robot. Thus, a deep understanding of the non-equilibrium behaviors of active polymer is of great significance for both biological physics and biomedical engineering [28].

Active polymer can be generally divided into two subclasses, i.e., polar and non-polar ones. For polar ac-

tive polymer like actin filament, active forces are along the backbone of the polymer, thus the total active force has a preferred direction [29–34]. This is different from the non-polar active polymer like active Brownian chain, where the active force on each monomer is uncorrelated [35–37]. Recently, it has been demonstrated that polar active polymer exhibits irreversible coil-to-globule transition without attraction, and the scaling exponent  $\nu$  gradually decreases from 0.588 and falls below 0.5 [38, 39]. Nevertheless, a general mechanism of the activity-induced conformation transition of polar active polymer still remains unknown.

In this letter, we systemically study the structure and dynamics of polar active polymers with controllable head activity. We find that the head activity plays a com-

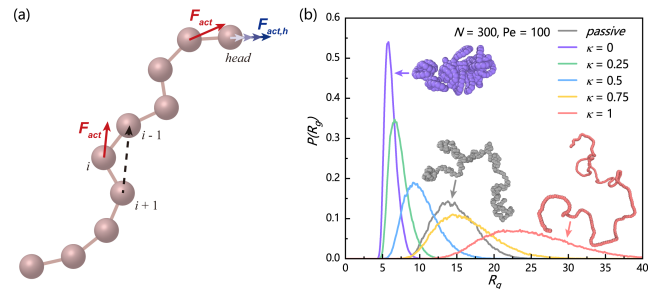


FIG. 1: (a) Schematics of polar active polymer, where red arrows represent active force on backbone monomers and blue arrows with gradient color denote tunable active force on the head monomer. (b) Probability distribution of radius of gyration  $P(R_g)$  for polymers with different head activity strength  $\kappa$ , where the insert shows corresponding chain configuration.

manding role for chain activity, resulting in re-entrant swelling of active polymer and non-monotonic variation of Flory exponent  $\nu$ , as well as the acceleration of polymer dynamics by an order of magnitude. These intriguing behaviours are results of the competition between two non-equilibrium effects (i.e. dynamic chain rigidity and the *involution* of chain configurations) arising from the head-controlled railway motion of active polymer. Moreover, we also identify several generic dynamic features of polar active polymers, i.e., a *linear* rather than exponential decay of the end-to-end vector correlation function, polymer-size dependent crossover from ballistic to diffusive dynamics, and a polymer-length independent diffusion coefficient that is sensitive to head activity. These novel dynamic phenomena are explained in a satisfactory dynamic theory based on railway motion.

**Model and simulations** As shown in Fig. 1a, we model the active polymer as a bead-spring chain of  $N$  monomers with bond length  $b$ . The excluded volume interaction and bond connecting are carefully chosen to guarantee conformation stability under self-driving conditions [30]. Based on [38], we assume the active force on backbone monomer  $i$  has a constant magnitude  $F_{act}$  and its direction polarizes to the head monomer ( $i=1$ ) along the local tangent determined by the nearest two monomers, i.e.,

$$\mathbf{F}_{act,i} = F_{act} \mathbf{e}_{i-1,i+1}, \quad i=2,3 \dots N-1, \quad (1)$$

with  $\mathbf{e}_{i,j} = (\mathbf{r}_i - \mathbf{r}_j) / |\mathbf{r}_i - \mathbf{r}_j|$ . The active force on tail monomer ( $i=N$ ) is set as  $\mathbf{F}_{act,N} = F_{act} \mathbf{r}_{N-1,N} / |\mathbf{r}_{N-1,N}|$ , while the active force on head monomer is controlled by the dimensionless head activity strength  $\kappa$ ,

$$\mathbf{F}_{act,1} = \kappa F_{act} \mathbf{r}_{1,2} / |\mathbf{r}_{1,2}|. \quad (2)$$

$\kappa$  can also be understood as the ratio between the head and backbone activities. The Péclet number  $Pe \equiv F_{act}b / (k_B T)$  is used to quantify the overall activity of the polymer, where  $k_B$  and  $T$  is the Boltzmann constant and temperature, respectively. Following Ref. [30] and [40], we set  $F_{act}b = \epsilon$  as the energy unit of the system, and adjust the Péclet number by changing thermal energy  $k_B T$ . The typical speed of active monomer is  $v_0 = F_{act} / \gamma$  with  $\gamma$  the friction coefficient. The unit time of the system is chosen as  $\tau_0 = b / v_0$ . We use standard Langevin dynamics to simulate the active polymer in free 3D space [30, 32, 34, 41]. More details about the model and simulations can be found in Supplemental Materials.

**Conformation of polar active polymers** We first show the probability distribution of radius of gyration  $P(R_g)$  for active polymer with various head activity under fixed  $Pe$  and  $N$  in Fig. 1b, where  $P(R_g)$  for passive polymer is also shown for comparison. In the absence of head activity ( $\kappa=0$ ), we find strong activity-induced

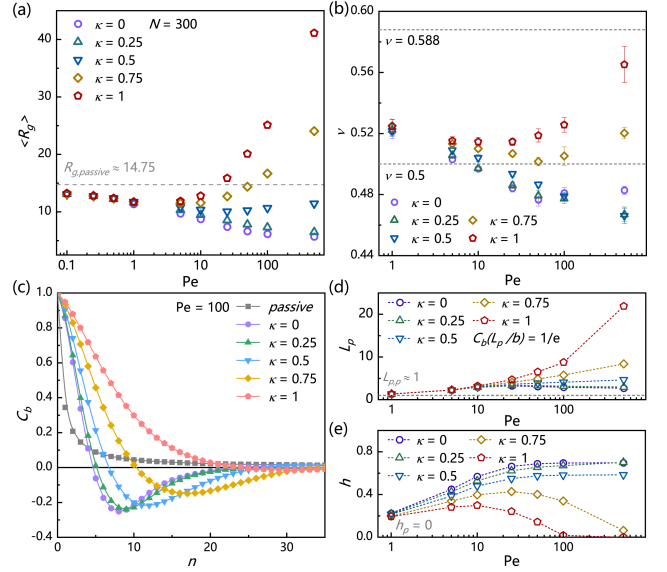


FIG. 2: (a) Average radius of gyration  $\langle R_g \rangle$  as a function of  $Pe$  under different head activity strength  $\kappa$ , where the gray dashed line represents passive polymer. (b) Flory exponent  $\nu$  as a function of  $Pe$ . (c) Bond-vector correlation function  $C_b(n)$  for passive polymer and active polymer under different  $\kappa$ . (d,e) Persistence length  $L_p$  and negative correlation strength  $h$  obtained from  $C_b(n)$  as a function of  $Pe$  under different  $\kappa$ .

collapse of the polymer chain, consistent with previous studies [38, 39]. However, with increasing head activity, active polymer gradually swells and becomes even more expanded than the passive polymer.

In Fig. 2a, we plot the average radius of gyration  $\langle R_g \rangle$  as a function of  $Pe$  under different  $\kappa$ , where  $\langle R_{g,passive} \rangle$  for passive polymer is drawn as a dashed line for comparison. For small head activity  $\kappa < 0.5$ , we find that  $\langle R_g \rangle$  shows monotonic decrease with increasing  $Pe$ . Nevertheless, for large head activity, an unusual non-monotonic behaviour of  $\langle R_g \rangle$  is observed with a first-stage shrinkage when  $Pe \lesssim 10$  and late-state expand at large  $Pe$ .

The Flory exponent  $\nu$  is obtained through plotting  $\langle R_g \rangle$  as a function of  $N$  (See Supplemental Fig. S2 for more data). In Fig. 2c, we show  $\nu$  as a function of  $Pe$  under different  $\kappa$  where the reference values of the random-walk chain ( $\nu=0.5$ ) and self-avoid walks chain ( $\nu=0.588$ ) are drawn as dashed lines. We find that under large head activity,  $\nu$  also exhibits a non-monotonic variation with increasing  $Pe$ , which indicates a fundamental change of fractal dimension of polymer configurations by head activity [1–3].

To explore these phenomena deeper, we calculate bond-vector correlation function  $C_b(n) = \langle \mathbf{b}_i \cdot \mathbf{b}_{i+n} / b_i^2 \rangle$ , with  $\mathbf{b}_i = \mathbf{e}_{i,i+1}$ . For typical semi-flexible polymers,  $C_b(n)$  decays exponentially. The characteristic correlation length  $n^*$  at which  $C_b(n^*)$  decays to  $e^{-1}$  defines the persistence length  $L_p = n^*b$ . In Fig. 2d, we plot  $C_b(n)$  for the passive polymer and active polymers with different  $\kappa$  under fixed  $Pe$ . We find that compared with passive

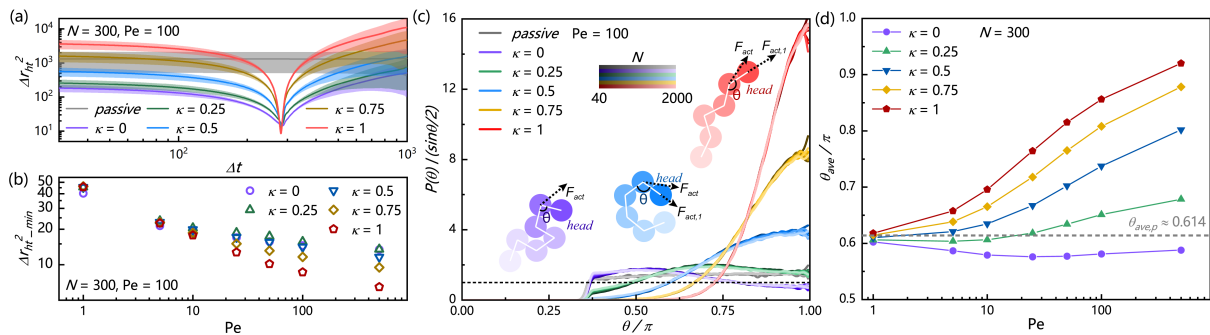


FIG. 3: (a) The correlation function of head-tail position  $\Delta r_{ht}^2(\Delta t)$  for polymer with different head activity, where the colored regions represent the error ranges. (b) The minimum value of  $\Delta r_{ht}^2$  as a function of  $Pe$ . (c) Probability distribution of the first angle  $P(\theta)$  normalized by  $\sin\theta/2$ . Insert: schematic representation of the first angle  $\theta$  and a simple mechanical analysis. (d) Averaged  $\theta$  as a function of activity  $Pe$ . In (a,c,e), the data for passive polymer are shown in gray color.

polymer,  $C_b(n)$  for active polymer with small  $\kappa$  shows a longer  $L_p$ , but with an abnormal negative correlation at intermediate length scale. This negative correlation indicates that the conformation of active polymer has a strong inward or involution tendency which is associated with the collapsed configuration. Nevertheless, this negative correlation is absent for passive polymer in bad solvent (Supplemental Fig. S3), which suggests a fundamental difference between these two systems, despite their apparent similarity. As  $\kappa$  grows, the persistence length increases significantly, with the negative correlation strength  $h$  decrease rapidly to zero. Here,  $h$  is defined as the area ratio between negative and positive regions in correlation function. Thus, active polymer with large head activity behaves similarly to that of passive semi-flexible chain. This emerging “dynamic rigidity” is a pure non-equilibrium effect, since the chain still remains mechanically flexible. Unlike semi-flexible passive chain, this dynamic rigidity alone can not predict the conformation of polymers. For example, Fig. 2d shows that even  $L_p$  is much larger than that of reference passive polymer,  $R_g$  is still smaller than  $R_{g,passive}$  due to a large negative correlation in  $C_b(n)$ .

We summarize the behaviors of persistence length  $L_p$  and  $h$  in Fig. 2d,e, respectively. One can see that with increasing  $Pe$ ,  $L_p$  remains around the low value and even decreases for polymer with small  $\kappa$ , but rises significantly for polymer with large  $\kappa$ , while  $h$  increases monotonically at small  $\kappa$  but exhibit strong non-monotonic behavior at large  $\kappa$ . Therefore, the activity of single head monomer determines the direction of overall active forces acting on the chain: for small head activity, the totally active driving is “inward”, corresponding to a large  $h$  (small  $L_p$ ) and a collapsed polymer state, while for large head activity, the totally active forces is “outward”, corresponding to a large  $L_p$  (small  $h$ ) and an extended polymer state.

**Head-controlled railway motion** The above abnormal conformation behaviors have a deep connection with the dynamic motion of active polymer. Since the

active propelling force is along the chain’s backbone, the active polymer adopts *active* reptation motion, which is also referred as “railway motion” [33] (see Supplemental Video S1-S5). To quantify such motion, we define a correlation function of head-tail position:

$$\Delta r_{ht}(\Delta t)^2 = \langle [\mathbf{r}_1(t) - \mathbf{r}_N(t + \Delta t)]^2 \rangle, \quad (3)$$

where the angle bracket represents the time and ensemble average. For perfect railway motion,  $\Delta r_{ht}^2$  decays to zero at time  $\tau_{ht} \simeq Nb/v_0 = N\tau_0$  and bounces back, which is the time for the tail to reach the original position of the head. For pure diffusive dynamics,  $\Delta r_{ht}^2$  will be a flat line determined by polymer’s mean squared end-to-end distance  $R_e^2$ . In Fig. 3a, we plot  $\Delta r_{ht}^2$  for active polymers with different  $\kappa$  under fixed  $Pe$ , where we find  $\Delta r_{ht}^2$  shows pronounce dips at the same  $\tau_{ht}$  independent of head activity. We further extract the minimal values  $\Delta r_{ht, min}^2$  which reflect the deviation from the perfect railway motion, and plot them as a function of  $Pe$  in Fig. 3b. We find that  $\Delta r_{ht, min}^2$  decreases with increasing  $Pe$ , which indicates polymer with a higher head activity  $\kappa$  shows relatively stronger railway motion.

For perfect railway motion chain, the direction of the head monomer is the only degree of freedom that determines the chain conformation. This direction can be represented by the bond angle  $\theta$  between the first three monomers. In Fig. 3c, we give the angle distribution  $P(\theta)$  for active polymers with different  $\kappa$  along with the passive polymer under varying polymer lengths. We find that for the active polymer without head activity, the peak of  $P(\theta)$  locates at small value around  $0.5\pi$  indicating the averaged bent configuration of polymer head. With increasing  $\kappa$ , the polymer head takes a more straight configuration. These results are independent of polymer length. Simple mechanical analysis in the insert of Fig. 3c shows that when the propulsion force of head monomer is smaller than the second monomers, the pushing force from back will induce a torque makes the bond  $\mathbf{r}_{1,2}$  bending inward. One the contrary, when the propulsion force of head monomer is large enough, head monomer will

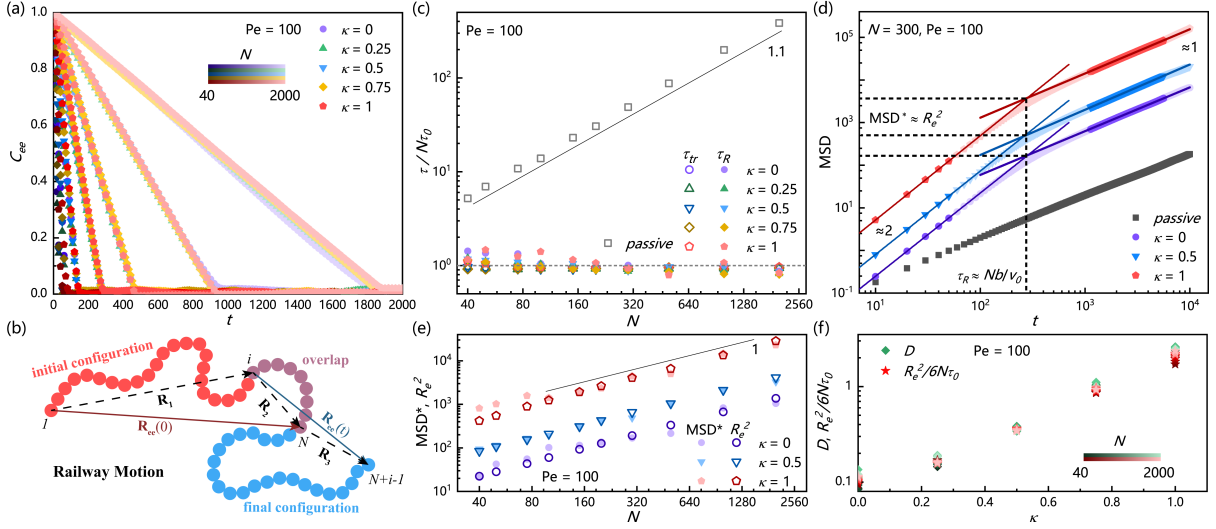


FIG. 4: (a) Correlation function of end-to-end vector  $C_{ee}$  decays linearly with time. (b) Schematics of the railway motion. (c) Relaxation time for end-to-end vector correlation  $\tau_{tr}$  and the critical dynamic transition time  $\tau_R$  as functions of chain length. The solid line is guide for eyes and the dashed line represents  $\tau = N\tau_0$ . (d) MSD( $t$ ) of polymers, where solid lines are linear fitting at different dynamic regimes and dashed lines indicate the critical MSD\* and  $\tau_R$ . (e) MSD\* and  $R_e^2$  as functions of chain length  $N$ . (f) Diffusion coefficient  $D$  and  $R_e^2/6N$  as functions of  $\kappa$  under different polymer lengths.

generate an opposite torque and pull the three monomers straight. For railway motion chain,  $P(\theta)$  determines the bond angle distribution of the whole chain. Thus, an increasing average  $\theta$  corresponds to an increasing persistence length  $L_p$  and a decreasing involution degree  $h$  of polymer. In Fig. 3d, we summarized the average value of  $\theta$ , which is qualitatively agreed with the behaviour of  $L_p$  and  $h$  in Fig. 2d,e.

**Dynamics of polar active polymers** To further explore the impact of head activity on the dynamics of polar active polymer, we calculate the end-to-end vector correlation function

$$C_{ee}(t) = \frac{\mathbf{R}_e(0) \cdot \mathbf{R}_e(t)}{\mathbf{R}_e(0)^2}, \quad (4)$$

and compare  $C_{ee}(t)$  for polymer under different head activity and polymer length  $N$  in Fig. 4a. A surprising finding is that all  $C_{ee}$  exhibit linear decay rather than exponential decay as for the passive polymer (Supplemental Fig. S4) [42, 43]. Moreover, we find  $C_{ee}(t)$  is intensive to the head activity  $\kappa$  and overall activity  $Pe$  but only depends on the chain length. In Fig. 4c, we plot the characteristic decay time  $\tau_{tr}$  of  $C_{ee}(t)$  as a function of  $N$ , we find all data from active polymer falling on the line  $\tau = N\tau_0$ . This behavior is distinct from the passive polymer for which  $\tau_{tr} \propto N^2$ .

Such abnormal dynamics can be explained theoretically based on railway motion of the polymer chain. As shown in Fig. 4b, assuming the initial and final configurations of polymer on the same “railway” have an overlap part with end-to-end vector  $\mathbf{R}_2$ , thus we have  $\mathbf{R}_e(0) = \mathbf{R}_1 + \mathbf{R}_2$  and  $\mathbf{R}_e(t) = \mathbf{R}_2 + \mathbf{R}_3$ , where  $\mathbf{R}_1$  and  $\mathbf{R}_3$

are the end-to-end vectors of the two non-overlapped parts. Since  $\mathbf{R}_1$ ,  $\mathbf{R}_2$ ,  $\mathbf{R}_3$  are statistically independent, we have  $\langle \mathbf{R}_i \cdot \mathbf{R}_j \rangle = 0$  for  $i \neq j$ . Combining the nearly linear dependence of  $\mathbf{R}_e^2$  on  $N$  shown in Fig. 4e, one can get

$$C_{ee}(t) \approx \frac{\mathbf{R}_2^2}{\mathbf{R}_e(0)^2} \approx \frac{Nb - v_0 t}{Nb} = 1 - \frac{t}{N\tau_0}, \quad t < N\tau_0, \quad (5)$$

which suggests  $\tau_{tr} = N\tau_0$ . Note that this result is independent of the shape of “railway” controlled by head activity.

The railway motion also results in novel polymer diffusion dynamics. One can prove that the displacement of center-of-mass of the polymer under railway motion can be written as

$$\Delta \mathbf{r}_{cm}(t) = \frac{1}{N\tau_0} \int_0^t \mathbf{R}_e(t) dt. \quad (6)$$

Thus, the mean square displacement (MSD) of polymer has the formation of (see SI for full derivation)

$$\text{MSD}(t) \equiv \Delta \mathbf{r}_{cm}^2(t) = \frac{1}{N^2 \tau_0^2} \int_0^t \int_0^t \mathbf{R}_e(t_1) \mathbf{R}_e(t_2) dt_1 dt_2 \simeq \begin{cases} \frac{R_e^2}{N^2 \tau_0^2} t^2, & t \ll N\tau_0 \\ \frac{R_e^2}{N\tau_0} t, & t \gg N\tau_0, \end{cases} \quad (7)$$

where  $|t_1 - t_2| < \tau_{tr}$  for the integration. Eq. (7) predicts a ballistic dynamics regime ( $\text{MSD} \sim t^2$ ) and a diffusion dynamics regime ( $\text{MSD} \sim t^1$ ) separated by the characteristic time  $\tau_R = N\tau_0$  and characteristic MSD\* ( $\tau_R$ )  $\simeq R_e^2$ .

In Fig. 4d, we plot the MSD(t) for active polymer with different  $\kappa$ , where the reference MSD(t) of passive polymer is shown in gray color. We find the simulation results agree well with our theoretical prediction. Especially  $\text{MSD}^*(\tau_R)$  match with  $R_e$  excellently when varying the polymer length (See Fig. 4e). Furthermore, based on Stokes-Einstein relation  $\text{MSD}=6Dt$  and Eq. (7), we can obtain the diffusion coefficient  $D=R_e^2/6N\tau_0$ . Since  $R_e^2\sim N$ , the diffusion coefficient is independent of chain length, which is in contrast with classical dynamic behavior  $D\sim\frac{1}{N}$  of passive Rouse chain [38, 44]. These predictions are also confirmed by the simulation results shown in Fig. 4f, at which  $D$  and  $R_e^2/6N\tau_0$  match very well under different  $\kappa$  and independent of  $N$ . At last, from Fig. 4f, one can see that the conformation and dynamics are coupled: the diffusion coefficient of an extended active polymer with large head activity can be an order of magnitude larger than the collapsed active polymer with small head activity. This provides us an efficient way to control the conformation and dynamics of active polymer, which may have application values in drug delivery and biomedical engineering [41, 45, 46].

**Conclusion** In conclusion, we find a general non-equilibrium mechanism that head activity commands the overall active forces on the polar active polymer performing railway motion, which leads to unusual conformation and dynamics behaviors of the polymer chain. We demonstrate that the low head activity favours bent head configuration, which causes a strong involution and the collapsing of polymer chain, while the high head activity helps the polymer straighten its head, resulting in an emerging “dynamic rigidity” and more extended chain conformation. The competition between the two non-trivial non-equilibrium effects leads to the re-entrant swelling of active polymer and non-monotonic variation of Flory exponent  $\nu$ . We also find many interesting dynamic features for polar active polymer, like a linear-decay of end-to-end vector correlation function  $C_{ee}$ , a polymer-size dependent crossover from ballistics to diffusion dynamics, as well as length-independent diffusion coefficient controlled by the head-activity. All these features are explained well by our dynamic theory. Our findings are not only essential for understanding the phase behaviors of more complicated active polymer fluids (e.g. cytoskeleton and bacterial DNA [47–49]), but also suggestive for designing efficient polymer-based drug delivery systems.

**Acknowledgments:** This work is supported by the National Natural Science Foundation of China (No.12104219).

- 
- \* lql@nju.edu.cn  
† myqiang@nju.edu.cn
- [1] P. G. De Gennes, *Scaling Concepts in Polymer Physics* (Cornell University Press, 1979).
  - [2] M. Doi and S. F. Edwards, *The Theory of Polymer Dynamics* (Oxford University Press: Oxford, 1988).
  - [3] M. Rubinstein and R. H. Colby, *Polymer Physics* (Oxford University Press: New York, 2003).
  - [4] P. J. Flory, *Principles of Polymer Chemistry* (Cornell University Press, Ithaca, NY, 1953).
  - [5] Y. Harada, A. Noguchi, A. Kishino, and T. Yanagida, *Nature*, **326**, 805 (1987).
  - [6] F. J. Nédélec, T. Surrey, A. C. Maggs, and S. Leibler, *Nature* **389**, 305 (1997).
  - [7] F. Jülicher, K. Kruse, J. Prost, and J. F. Joanny, *Phys. Rep.* **449**, 3 (2007).
  - [8] N. M. Stano, Y. J. Jeong, I. Donmez, P. Tummalapalli, M. K. Levin, and S. S. Patel, *Nature* **435**, 370 (2005).
  - [9] D. E. Kim, M. Narayan, and S. S. Patel, *J. Mol. Biol.* **321**, 807 (2002).
  - [10] J. L. Liu, *Annu. Rev. Cell Dev. Biol.* **32**, 349 (2016).
  - [11] H. Li, F. Ye, J. Y. Ren, P. Y. Wang, L. L. Du, and J. L. Liu, *FASEB J.* **32**, 5891 (2018).
  - [12] T. Surrey, F. Nédélec, S. Leibler, and E. Karsenti, *Science* **292**, 1167 (2001).
  - [13] V. Schaller, C. Weber, E. Frey, and A. R. Bausch, *Soft Matter* **7**, 3213 (2011).
  - [14] G. A. Vliegenthart, A. Ravichandran, M. Ripoll, T. Auth, and G. Gompper, *Sci. Adv.* **6**, 1 (2020).
  - [15] J. M. Moore, T. N. Thompson, M. A. Glaser, and M. D. Betterton, *Soft Matter* **16**, 9436 (2020).
  - [16] R. Adkins, I. Kolvin, Z. You, S. Witthaus, M. C. Marchetti, and Z. Dogic, *Science* **377**, 768 (2022).
  - [17] L. Natali, L. Caprini, and F. Cecconi, *Soft Matter* **16**, 2594 (2020).
  - [18] X.-Z. Cao, H. Merlitz, C.-X. Wu, and M. G. Forest, *Phys. Rev. E* **106** (2022).
  - [19] V. Schaller, C. Weber, C. Semmrich, E. Frey, and A. R. Bausch, *Nature* **467**, 73 (2010).
  - [20] Y. Sumino, K. H. Nagai, Y. Shitaka, D. Tanaka, K. Yoshikawa, H. Chaté, and K. Oiwa, *Nature* **483**, 448 (2012).
  - [21] R. Dreyfus, J. Baudry, M. L. Roper, M. Fermigier, H. A. Stone, and J. Bibette, *Nature* **437**, 862 (2005).
  - [22] L. J. Hill, N. E. Richey, Y. Sung, P. T. Dirlam, J. J. Griebel, E. Lavoie-Higgins, I. B. Shim, N. Pinna, M. G. Willinger, W. Vogel, J. J. Benkoski, K. Char, and J. Pyun, *ACS Nano* **8**, 3272 (2014).
  - [23] B. Biswas, R. K. Manna, A. Laskar, P. B. Kumar, R. Adhikari, and G. Kumaraswamy, *ACS Nano* **11**, 10025 (2017).
  - [24] D. Nishiguchi, J. Iwasawa, H. R. Jiang, and M. Sano, *New J. Phys.* **20** (2018).
  - [25] H. Massana-Cid, F. Martinez-Pedrero, E. Navarro-Argemí, and I. Pagonabarraga, *New J. Phys.* **19**, 103031 (2017).
  - [26] L. Zhang, J. J. Abbott, L. Dong, B. E. Kratochvil, D. Bell, and B. J. Nelson, *Appl. Phys. Lett.* **94**, 2007 (2009).
  - [27] L. Zhang, J. J. Abbott, L. Dong, K. E. Peyer, B. E. Kratochvil, H. Zhang, C. Bergeles, and B. J. Nelson, *Nano*

- Lett. **9**, 3663 (2009).
- [28] R. G. Winkler, J. Elgeti, and G. Gompper, *J. Phys. Soc. Japan* **86**, 1 (2017).
- [29] H. Jiang and Z. Hou, *Soft Matter* **10**, 1012 (2014).
- [30] E. Locatelli, V. Bianco, and P. Malgaretti, *Phys. Rev. Lett.* **126**, 97801 (2021).
- [31] Z. Mokhtari and A. Zippelius, *Phys. Rev. Lett.* **123**, 28001 (2019).
- [32] K. R. Prathyusha, S. Henkes, and R. Sknepnek, *Phys. Rev. E* **97**, 1 (2018).
- [33] R. E. Isele-Holder, J. Elgeti, and G. Gompper, *Soft Matter* **11**, 7181 (2015).
- [34] A. Shee, N. Gupta, A. Chaudhuri, and D. Chaudhuri, *Soft Matter* **17**, 2120 (2021).
- [35] A. Kaiser, S. Babel, B. Ten Hagen, C. Von Ferber, and H. Löwen, *J. Chem. Phys.* **142** (2015).
- [36] T. Eisenstecken, G. Gompper, and R. G. Winkler, *J. Chem. Phys.* **146** (2017).
- [37] S. K. Anand and S. P. Singh, *Phys. Rev. E* **101**, 1 (2020).
- [38] V. Bianco, E. Locatelli, and P. Malgaretti, *Phys. Rev. Lett.* **121**, 217802 (2018).
- [39] N. Jain and S. Thakur, *Macromolecules* **55**, 2375 (2022).
- [40] J. Stenhammar, D. Marenduzzo, R. J. Allen, and M. E. Cates, *Soft Matter* **10**, 1489 (2014).
- [41] R. E. Isele-Holder, J. Jäger, G. Saggiorato, J. Elgeti, and G. Gompper, *Soft Matter* **12**, 8495 (2016).
- [42] R. Azuma and H. Takayama, *J. Chem. Phys.* **111**, 8666 (1999).
- [43] R. Descas, J. U. Sommer, and A. Blumen, *J. Chem. Phys.* **120**, 8831 (2004).
- [44] A. R. Tejedor and J. Ramírez, *Macromolecules* **52**, 8788 (2019).
- [45] Y. Sasaki, Y. Takikawa, V. S. Jampani, H. Hoshikawa, T. Seto, C. Bahr, S. Herminghaus, Y. Hidaka, and H. Orihara, *Soft Matter* **10**, 8813 (2014).
- [46] H. D. Vuijk, H. Merlitz, M. Lang, A. Sharma, and J.-U. Sommer, *Phys. Rev. Lett.* **126**, 208102 (2021).
- [47] G. Danuser, J. Allard, and A. Mogilner, *Annu. Rev. Cell Dev. Biol.* **29**, 501 (2013).
- [48] M. Murrell, P. W. Oakes, M. Lenz, and M. L. Gardel, *Nat. Rev. Mol. Cell Biol.* **16**, 486 (2015).
- [49] D. A. Fletcher and R. D. Mullins, *Nature* **463**, 485 (2010).